

**Low-cost fermions in classical field simulations**

Sz. Borsányi\* and M. Hindmarsh†

*Department of Physics and Astronomy, University of Sussex, Brighton, East Sussex BN1 9QH, United Kingdom*

(Received 17 October 2008; published 11 March 2009)

We discuss the possible extension of the bosonic classical field theory simulations to include fermions. This problem has been addressed in terms of the inhomogeneous mean-field approximation by Aarts and Smit. By performing a stochastic integration of an equivalent set of equations we can extend the original  $1 + 1$  dimensional calculations so that they become feasible in higher dimensions. We test the scheme in  $2 + 1$  dimensions and discuss some classical applications with fermions for the first time, such as the decay of oscillons.

DOI: [10.1103/PhysRevD.79.065010](https://doi.org/10.1103/PhysRevD.79.065010)

PACS numbers: 03.65.Pm, 11.15.Kc

**I. INTRODUCTION**

Since the advent of modern computational facilities classical field theory is one of the most popular approaches to nonequilibrium field theory. The classical approximation to a quantum field theory is well justified in several cosmological applications ranging from reheating of the postinflationary Universe [1,2] followed by an evolution through various phase transitions [3] to the nonlinear evolution of the hypothetical cosmic strings [4–6]. Classical methods have also received an increasing amount of attention from the heavy ion community. The initial evolution of the highly excited gluon plasma in little-bang experiments turns out to be well modeled by classical Yang-Mills equations [7].

The preheating of the inflationary Universe was one of the pioneering applications of the nonlinear classical wave equations [8]. In the mostly studied chaotic and hybrid inflation scenarios the nonlinear dynamics is driven by an instability, which is parametric or tachyonic, respectively. Instabilities lead to nonperturbatively large occupation numbers, which is a prerequisite for the classical approximation, but it also requires a nonperturbative treatment, which is the actual strength of the classical equations. The classical simulations of preheating can make estimates on non-Gaussian density perturbations [9] as well as on the production of gravitational waves [10–12] and primordial magnetic fields [13].

Nonperturbative methods are especially useful when dealing with nonequilibrium phase transitions in the early Universe [14]. A typical example where the fields are required to be out of equilibrium is baryogenesis. A second strength of the classical approximation is that equilibrium is not a prerequisite. Solving the real time Yang-Mills equations with far-from-equilibrium initial conditions, one could gain access to the evolution of the Chern-Simons number [15–17]. For this to be accomplished, the third strength of the classical equations has been exploited:

its preservation of gauge invariance under time-independent transformations.

The fourth strength of the classical approach is its simplicity and cheap implementation even at large scales. This feature makes it an excellent tool for studying topological defects, especially the hypothetical network of cosmic strings. To address formation and evolution of defect networks very different length scales have to be properly incorporated into one numerical computation. This situation is getting worse in an expanding universe, but in the classical setting these calculations are still affordable [18]. In principle, one could take the zero-width limit and solve the Nambu-Goto equations [19]. For fundamental strings this is a natural procedure, but for strings which are topological defects, microscopic physics plays a significant role in the decay mechanism of strings [20]. Explicit calculations have been made in the context of gauge strings in the Abelian Higgs model [18,20,21], global [22] and semilocal strings [23,24], as well as domain walls [25,26]. The relevance of these calculations has been recently highlighted by the discovery of possible traces of cosmic strings in the cosmic microwave background [24,27].

Classical field theory simulations are not only used for cosmology: In heavy ion collisions, the early evolution of the gluon plasma can be described by classical Yang-Mills equations [7]. This facilitates a nonperturbative description of the glasma, i.e. the intermediate state after the melting of the color glass condensate prior to thermalization to quark gluon plasma [28,29]. The produced non-Abelian plasma is highly anisotropic, and as such, it is subject to instabilities [30]. Classical methods have proved very useful for giving a quantitative account on the isotropization driven by these Weibel instabilities [31,32]. Alternatively, one can replace the hard sector of the field theory by classical particles represented by a set of Vlasov equations on the background of soft classical fields [33,34].

Finally, we point out that the ergodicity of the classical field trajectories makes the classical simulations an essential and robust method for studying thermal classical lattice systems in real time. In statistical field theory one averages over an ensemble of initial field configurations and ob-

\*s.borsanyi@sussex.ac.uk

†m.b.hindmarsh@sussex.ac.uk

serves, e.g., the real-time dynamics of symmetry breaking [35], with possible formation of quasi-stable localized excitations, dubbed oscillons [36]. The presence of long-lived oscillons induces resonant nucleation, and they become a driving force of first order phase transitions [37].

The classical approximation has severe limitations, however. The continuum equilibrium theory is plagued by Rayleigh-Jeans divergences, and a renormalization with local counterterms is not possible, in general [38]. Moreover, the counterterms are temperature dependent, which makes a consistent out-of-equilibrium renormalization impossible. This means that classical theories need an intrinsic cutoff scale, which, in practice, sets the spacing of the lattice discretization. From whatever initial ensemble of classical fields the straightforward integration of the Euler-Lagrange equations of the theory brings the systems towards an equilibrium defined by the classical Hamiltonian. This equilibrium differs from a true quantum thermal state, but the difference is negligible for soft modes and only affects hard excitations. In terms of particle numbers, a system is considered in the classical domain if the occupancy is sufficiently high. The infrared physics, which is mostly sensitive to nonperturbative phenomena, is usually not vulnerable to quantum effects, but on the ultraviolet end of the spectrum one has to balance between discretization errors and miscalculated hard degrees of freedom. Even if we start from an infrared dominated initial condition, hard modes are becoming increasingly dominant on the course of thermalization and the classical system automatically leaves its domain of validity.

There is another first principles approach to nonequilibrium field theory, which shares none of the aforementioned shortcomings. It has been numerically demonstrated that even a low order truncation of the two-particle irreducible (2PI) effective action yields equations of motion, capable of describing irreversible quantum dynamics, including thermalization [39]. This powerful resummation technique can be directly applied to relevant problems in cosmology [40,41] or in hot Abelian gauge theories [42,43], as well as in the many-body theory of ultracold condensates [44]. Yet, for non-Abelian gauge fields the more complete 3PI resummation becomes necessary [45,46], and for a setting with topological defects an inhomogeneous treatment is inevitable [47]. Both extensions are expensive, so in these cases we will have to fall back to the classical approximation and use 2PI to benchmark it where their domains of validity overlap. These precision tests in the  $O(N)$  scalar model had the reassuring result that particle numbers as small as  $\sim 10$  already put the system into the classical domain [48,49].

There is, however, another important deficiency of the classical approximation. All the applications listed in the previous paragraphs were entirely limited to bosonic fields. Classical simulations of both baryogenesis and heavy ion collisions could benefit from a direct modeling of quarks, if that were feasible.

As dimensional reduction suggests, fermionic fields are purely quantum degrees of freedom, just like the nonstatic components of a bosonic field theory. The classical field theory does have bosonic fluctuations, and in the absence of quantum degrees of freedom, bosonic particle production is automatically modeled as the excitation of the fluctuating background. The analogous production of fermions, however, is not mapped onto any existing degree of freedom.

The inclusion of fermions is rather trivial in the 2PI framework, where bosonic quantum fluctuations interact with fermionic quantum fluctuations, and an explicit calculation has been presented to show the real-time simultaneous onset of Fermi-Dirac and Bose-Einstein distributions [50]. However, when dealing with non-Abelian gauge fields, or strong inhomogeneities, we will need to resort to some extension of the classical theory. This extension is the actual topic of this paper.

In this paper, we build on the ideas of Aarts and Smit [51,52] and by “integrating the fermion determinant” we solve an effective theory for the classical scalar background. We go beyond the recent applications in Refs. [53,54] by including the backreaction in our calculation. Our efficient solution technique enables us to go beyond  $1 + 1$  dimensions in the simulations.

In Sec. II, we review the standard description of the fermionic fluctuations. Then in Sec. III, we introduce a stochastic approach, which provides us a more efficient algorithm than the so far known mode function expansion. In Sec. IV, we investigate the capabilities of this semiclassical approximation for describing irreversible phenomena, such as damping and thermalization. We continue with a bit more exotic application involving oscillons in Sec. V and discuss the possible future applications of this semiclassical scheme in Sec. VI. The spinor representations that we actually used in our numerics we give in Appendix A. In a naively discretized lattice field theory the number of fermion flavors is doubled in each space-time direction. We discuss the possible elimination of the extra flavors in Appendix B.

## II. INTEGRATING THE FERMION DEGREE OF FREEDOM

### A. A scalar model with fermions

Let us pick a simple scalar model coupled to a fermion flavor through Yukawa interaction:

$$\mathcal{L} = \frac{1}{2} \partial\Phi^* \partial\Phi - V(\Phi) + \sum_k [i\bar{\Psi}_k \gamma^\mu \partial_\mu \Psi_k - \bar{\Psi}_k (MP_L + M^*P_R)\Psi_k]. \quad (1)$$

Here the  $M$  complex fermion mass is a function of the background:

$$M(x) = m - g\Phi(x). \quad (2)$$

The projectors are defined as  $P_L = \frac{1}{2}(1 - \gamma^5)$  and  $P_R = \frac{1}{2}(1 + \gamma^5)$ . The index  $k$  runs over  $N_f$  identical fermion flavors. We will not use any of the special features of the bosonic sector, and our discussion below will also apply to classical lattice gauge theories with a covariant coupling to fermions.

Before going into details we summarize our strategy by defining a bosonic effective action  $\Gamma[\Phi]$  as

$$e^{i\Gamma[\Phi]} = \int \prod_k D\Psi_k^+ D\Psi_k e^{i \int \mathcal{L}(\Phi, \Psi^+, \Psi)}. \quad (3)$$

Our goal is to solve the semiclassical equation of motion  $\delta\Gamma[\Phi]/\delta\Phi = 0$  without further approximation. This path integral has to be understood on a real-time contour with a forward and backward time branch. The contour ends at (zero) initial time where it connects to the initial density operator. We will use the perturbative vacuum or many-particle state as an initial condition.

The Dirac equation written for the spinor operators is linear

$$(i\gamma^\mu \partial_\mu - m + g \operatorname{Re}\Phi(x) - ig \operatorname{Im}\Phi(x)\gamma^5)\Psi(x) = 0, \quad (4)$$

$$i\partial_\mu \bar{\Psi}(x)\gamma^\mu + \bar{\Psi}(x)(m - g \operatorname{Re}\Phi(x) + ig \operatorname{Im}\Phi(x)\gamma^5) = 0, \quad (5)$$

which manifests on the level of diagrams in the simple rule that fermion propagator lines never cross. The interaction is mediated by the bosonic field, which is modeled by a fluctuating background.

Instead of using anticommuting operators we rewrite the Dirac equation so that it applies to the symmetrized two-point function:

$$(i\gamma^\mu \partial_{x,\mu} - m + g \operatorname{Re}\Phi(x) - ig \operatorname{Im}\Phi(x)\gamma^5)D(x, y) = 0, \quad (6)$$

$$i\partial_{y,\mu} D(x, y)\gamma^\mu + D(x, y)(m - g \operatorname{Re}\Phi(y) + ig \operatorname{Im}\Phi(y)\gamma^5) = 0, \quad (7)$$

where  $D(x, y)$  is defined as

$$D(x, y)_{ij} = \frac{1}{2}(D_{ij}^>(x, y) - D_{ij}^<(x, y)) = \frac{1}{2}\langle[\Psi_i(x), \bar{\Psi}_j(y)]\rangle, \quad (8)$$

$$D^<(x, y)_{ij} = \langle\bar{\Psi}_j(y)\Psi_i(x)\rangle, \quad (9)$$

$$D^>(x, y)_{ij} = \langle\Psi_i(x)\bar{\Psi}_j(y)\rangle, \quad (10)$$

where  $i, j$  represent the Dirac as well as flavor indices. The propagator  $D$  is identical to the  $F$ -type two-point function in the literature of nonequilibrium Green's functions as well as in Ref. [50]. One can work out an equation for the spectral function as well, which will take an identical form.

The bosonic background obeys a simple wave equation,

$$\partial_x^2 \Phi(x) + V'(\Phi(x)) + N_f J(x) = 0, \quad (11)$$

where the fermionic backreaction is carried by the current  $J$ , which is a combination of the scalar and pseudoscalar currents:

$$J(x) = J^S(x) + J^{\text{PS}}(x) = 2g \operatorname{Tr}D(x, x)P_R, \quad (12)$$

$$J^S(x) = -g\langle\bar{\Psi}(x)\Psi(x)\rangle = g \operatorname{Tr}D(x, x), \quad (13)$$

$$J^{\text{PS}}(x) = -g\langle\bar{\Psi}(x)\gamma^5\Psi(x)\rangle = g \operatorname{Tr}D(x, x)\gamma^5. \quad (14)$$

The scalar current is always real; the pseudoscalar current is always imaginary.

In a theory with a Dirac mass  $m$  the vacuum propagator takes the following form:

$$D(x^0, \vec{x}, y^0, \vec{y})|_{x^0=y^0} = \int_{\vec{p}} e^{-ip_j(x^j-y^j)} \frac{m + p_i\gamma^i}{2\omega_{\vec{p}}}, \quad (15)$$

with  $\omega_{\vec{p}}^2 = m^2 + |\vec{p}|^2$ . The Latin indices refer to space only. In this equation we introduced the notation  $\int_{\vec{p}}$  for the three-dimensional momentum integral  $\int d^3p/(2\pi)^3$ .

In many cases when one inquires about the fermion production the vacuum initial condition is used, preferably. Since Eqs. (6) and (7) are first order in time, all further evolution is determined, once the background is known. Of course, any other initial particle content is also feasible, one can, e.g., set an uneven number of particles and antiparticles, which is the microcanonical analog of a baryochemical potential. We will give formulas where these particle numbers enter later below.

## B. Mode function expansion

One can solve Eqs. (6), (7), and (11) numerically without any further information. The standard strategy is to introduce mode functions, i.e. to treat time evolution as a Bogolyubov transformation of the initial-time ladder operator. This method has been formerly used for bosonic fluctuations on a homogeneous background [55–57], and later extended to fermionic systems [58–60] and also to inhomogeneous backgrounds [61,62]. The equations for fermionic fluctuations on an inhomogeneous backgrounds have been worked out in detail by Aarts and Smit [51].

We introduce the mode functions  $\phi^{u,s}(x, \vec{p})$  and  $\phi^{v,s}(x, \vec{p})$  as classical solutions weighting the anticommuting ladder operators with

$$\{b_s(\vec{p}), b_{s'}^+(\vec{q})\} = (2\pi)^3 \delta(\vec{p} - \vec{q}) \delta_{s,s'}, \quad (16)$$

$$\{d_s(\vec{p}), d_{s'}^+(\vec{q})\} = (2\pi)^3 \delta(\vec{p} - \vec{q}) \delta_{s,s'} \quad (17)$$

in the fermion field operator:

$$\Psi(x) = \int_{\vec{p}} \sum_s (b_s(\vec{p}) \phi^{u,s}(x, \vec{p}) + d_s^+(\vec{p}) \phi^{v,s}(x, -\vec{p})). \quad (18)$$

We introduced the spinor index  $s$  that runs from 1 to 2. If the fermions' initial condition is homogeneous, one has

$$\phi^{u,s}(x, \vec{p})|_{x^0=0} = u^s(\vec{p}) e^{-ip_j x^j}, \quad (19)$$

$$\phi^{v,s}(x, \vec{p})|_{x^0=0} = v^s(\vec{p}) e^{-ip_j x^j}. \quad (20)$$

The ladder operators correspond to these initial-time excitations that are transformed as fermions travel through the background. The statistical features of these operators actually reflect the initial particle distribution:

$$\langle [b^s(\vec{p}), b^{s'+}(\vec{q})] \rangle = (2\pi)^3 \delta(\vec{p} - \vec{q}) \delta_{s,s'} (1 - 2n_+^s(\vec{p})), \quad (21)$$

$$\langle [d^s(\vec{p}), d^{s'+}(\vec{q})] \rangle = (2\pi)^3 \delta(\vec{p} - \vec{q}) \delta_{s,s'} (1 - 2n_-^s(\vec{p})). \quad (22)$$

The  $u^s(\vec{p})$  and  $v^s(\vec{p})$  spinors in Eq. (20) are defined as the eigenvectors of the vacuum correlation matrix written momentum space:

$$\mathcal{M}(\vec{p}) = \frac{1}{\omega_{\vec{p}}} (p_i \gamma^i \gamma^0 + m \gamma^0). \quad (23)$$

This matrix has the eigenvalues  $(+1, +1, -1, -1)$  corresponding to the eigenvectors  $u^1(\vec{p})$ ,  $u^2(\vec{p})$ ,  $v^1(\vec{p})$ , and  $v^2(\vec{p})$ , respectively. On a nontrivial background these eigenvalues disambiguate between particle and antiparticle solutions. Using the identities

$$\gamma^0 v^s(-\vec{p}) = v^s(\vec{p}), \quad (24)$$

$$\sum_s (u^s(\vec{p}) u^{s+}(\vec{p}) + v^s(\vec{p}) v^{s+}(\vec{p})) = 1, \quad (25)$$

$$\sum_s (u^s(\vec{p}) u^{s+}(\vec{p}) - v^s(\vec{p}) v^{s+}(\vec{p})) = \mathcal{M} \vec{p}, \quad (26)$$

one can show that at initial time the two-point function in Eq. (15) is correctly reproduced by the field operator in Eq. (18).

At any later  $x_0$  the mode functions are given by the following commutators:

$$\langle [\Psi(x), b^{s+}(\vec{p})] \rangle = \phi^{u,s}(x, \vec{p}), \quad (27)$$

$$\langle [\Psi(x), d^s(-\vec{p})] \rangle = -\phi^{v,s}(x, \vec{p}). \quad (28)$$

On the other hand, one can express the ladder operators in terms of the initial-time field operator by

$$b^{s+}(\vec{p}) = \int_{\vec{x}} \Psi^+(x)|_{x_0=0} u^s(\vec{p}) e^{-i\vec{p}\cdot\vec{x}}, \quad (29)$$

$$d^s(-\vec{p}) = \int_{\vec{x}} \Psi^+(x)|_{x_0=0} v^s(\vec{p}) e^{-i\vec{p}\cdot\vec{x}}. \quad (30)$$

Using these one has

$$\phi^{u,s}(x, \vec{p}) = 2 \int_{\vec{p}} e^{-i\vec{p}\cdot\vec{y}} D(x, y)|_{y_0=0} \gamma^0 u^s(\vec{p}), \quad (31)$$

$$\phi^{v,s}(x, \vec{p}) = -2 \int_{\vec{p}} e^{-i\vec{p}\cdot\vec{y}} D(x, y)|_{y_0=0} \gamma^0 v^s(\vec{p}). \quad (32)$$

These equations relate the propagators used in Eqs. (6) and (7) to the mode functions. So that  $\Psi(x)$  in Eq. (18) solves the Dirac equation (4) the mode functions  $\phi^{u,s}(x, \vec{p})$  as well as  $\phi^{v,s}(x, \vec{p})$  have to solve the same Dirac equation for all  $\vec{p}$  and  $s$ .

$$(i\gamma^\mu \partial_\mu - m + g \text{Re}\Phi(x) - ig \text{Im}\Phi(x) \gamma^5) \phi^{u/v,s}(x, \vec{p}) = 0. \quad (33)$$

This is now also manifest from Eq. (32). We can actually confirm the initial condition in Eq. (20) by inserting  $D(x, y)$  of Eq. (15) into Eq. (32).

### C. Renormalization

The effective potential in Eq. (3) has a nonpolynomial contribution from the logarithm of the fermion determinant. Expanding in  $\Phi$  to  $n$ -th order one finds the fermion one-loop diagrams with  $n$  external bosonic lines. These diagrams with  $n \leq 4$  are potentially divergent in  $3 + 1$  dimensions. Already at  $n = 1$ , the source (12) is quadratically divergent.

We renormalize the scalar potential additively by introducing a renormalized potential  $V$  and a counterfunction  $\delta V'(\Phi)$  in Eq. (11). We also introduce a wave function renormalization so that the renormalized scalar evolution equation reads

$$Z \partial_x^2 \Phi_R(x) + V'_R(\Phi_R(x)) + \delta V'(\Phi_R(x)) + N_f J(x) = 0. \quad (34)$$

To calculate  $\delta Z = Z - 1$  we linearize  $J$  in  $\Phi$  and obtain

$$\begin{aligned} & Z \partial_x^2 \Phi_R(x) + V'_R(\Phi_R(x)) + \delta V'(\Phi_R(x)) \\ &= N_f \int_0^{x_0} dz_0 \int d^3 z \Sigma(x-z) \Phi_R(z). \end{aligned} \quad (35)$$

Here  $\Sigma(x)$  stands for the vacuum one-loop self-energy. The counterterms  $\delta Z$  and  $\delta \mu^2$  [see Eq. (40) below] will be set so that they cancel the potentially divergent first two coefficients in the  $k^2$  expansion of  $\Sigma(k_0, \vec{k})$  so that the renormalized self-energy

$$\Sigma_R = \delta Z k^2 + \delta m^2 + \Sigma(k_0, \vec{k}) \quad (36)$$

is finite in the perturbative vacuum of the fermions.

Following the existing practice in classical simulations, we will use a temporal discretization step that is negligible

to the spatial lattice spacing, i.e the cutoff is three dimensional, and the three-dimensional momentum integrals are implicitly regularized. We give an explicit form of  $\Sigma$  in the spatial Fourier space:

$$\begin{aligned} \Sigma(t, \vec{k}) &= -4g^2 \int_{\vec{p}} \left[ \frac{m^2 - \vec{p}(\vec{p} - \vec{k})}{\omega_{\vec{p}} \omega_{\vec{k}-\vec{p}}} - 1 \right] \\ &\times \sin \omega_{\vec{p}} t \cos \omega_{\vec{k}-\vec{p}} t. \end{aligned} \quad (37)$$

We define  $\omega_{\vec{p}} = \sqrt{m^2 + p^2}$ . The wave function renormalization we either get by taking the second  $k$  derivative at scale of renormalization, which is  $k = 0$  in our calculation, or one calculates it from the real-time behavior using the formula

$$\delta Z = N_f \int_0^\infty dt \frac{t^2}{2} \Sigma(t, \vec{k})|_{\vec{k}=0}. \quad (38)$$

This equation is the real-time variant of  $\delta Z = N_f \partial^2 \Sigma(k_0, \vec{k}) / (\partial k_0)^2$  at zero momentum and makes sure that the coefficient of  $k^2$  vanishes in Eq. (36).

One can perform the time integral in Eq. (38) under the assumption that oscillations of the indeterminate integral at large times are incoherent and they are averaged away when the  $\vec{k}$  integral is carried out. One finally arrives at

$$\delta Z = -\frac{N_f g^2}{2} \int_{\vec{p}} \frac{p^2}{\omega_{\vec{p}}^5}; \quad (39)$$

the divergence is logarithmic, as expected. An analogous calculation delivers the scalar mass counterterm

$$\delta \mu^2 = \int_0^\infty dt \Sigma(t, \vec{k})|_{\vec{k}=0} = 2N_f g^2 \int_{\vec{p}} \frac{p^2}{\omega_{\vec{p}}^3}, \quad (40)$$

which is quadratically divergent.

To renormalize the coupling we need to go beyond the linear approximation in Eq. (35). We renormalize the effective potential at zero momentum. We analyze the nonlinear response to a static field and compensate the force on this static field by  $\delta V'$ . This way we do more than subtracting divergences. We actually alter the finite part of the theory so that the scalar potential is exactly as it was before coupling to fermions. This complete renormalization will ensure the correctness of any comparison with the purely bosonic classical field theory.

A static scalar field with a Yukawa coupling is similar to a Dirac mass. The current  $J$  is then constant in space and time, but it depends on the mass  $M = m - g\Phi_R$ . The counterterm  $\delta V'(\Phi_R)$  based on the vacuum one-loop diagrams reads

$$\delta V'(\Phi_R) = -2N_f g \int_{\vec{p}} \frac{m - g\Phi_R}{\sqrt{(m - g\Phi_R)^2 + p^2}}. \quad (41)$$

Expanding this integral to linear order in  $\Phi$  gives the same counterterm as we have already found in Eq. (40). To third order in  $\Phi$  we find in the chiral limit for the coupling renormalization  $\delta\lambda = 12\delta Z$  as it has been also derived in [58].

Of course, the integral in Eq. (41) would be very time consuming to calculate in each space-time point when solving Eq. (34). Therefore we approximate  $\delta V'$  with a 15th order polynomial fitted in the range  $ag\Phi \in [-2.5, 2.5]$ . The relative precision of the fit is between 1% and 10%, (the greatest when  $\Phi_R \approx 0$ ). The fit interval is exceeded only by extreme excitations on coarse lattices, and one can extend it with little effort.

In the rest of the paper we do not write out the  $R$  index for the renormalized background, and all parameters are understood as renormalized. For simplicity, we also hide the counterterms in the equations we discuss, but we keep them in our numerics, of course.

Contrary to Ref. [58], in this approach we solve equations with divergences, which cancel in the end result. This makes the final removal of the cutoff impossible, and such a calculation is usually error prone close to the continuum limit. But in this case we solve a lattice field theory classically and it makes no sense to even approach the continuum limit. This renormalization makes sure that the fermionic vacuum does not alter the bosonic vacuum, but the classical divergences from the closed bosonic loops are as dangerous as before.

By construction, fermions have now no impact on a static bosonic field, but there is a damping rate for dynamical fields, which is given in the real scalar case by

$$\gamma(k) = \frac{1}{2k_0} \int_0^\infty dt \sin(k_0 t) \Sigma(t, \vec{k}). \quad (42)$$

For a scalar with mass  $\mu$  this evaluates for homogeneous mode to

$$\begin{aligned} \gamma(\mu, \vec{k})|_{\vec{k}=0} &= \frac{g^2 N_f \pi}{2\mu} \int_{\vec{p}} \delta(\mu/2 - \omega_p) \\ &= \frac{g^2 N_f}{16\pi \mu^2} (\mu^2 - 4m^2)^{3/2}, \end{aligned} \quad (43)$$

if  $\mu > 2m$ . The damping rate is directly observable from the numerics. Since it is proportional to  $N_f$ , it facilitates the measurement of the number of doublers in a lattice implementation.

### III. STOCHASTIC APPROACH

In Eq. (33) of the previous section a separate field has to be evolved for each mode  $\vec{p}$  and spinor index. On a three-dimensional lattice with  $N^3$  sites this means a coupled set of  $4 \cdot 4 \cdot N^6$  complex ordinary differential equations. This relatively high price might explain the fact that in nearly

ten years time since the equations have been published no calculation has been carried out beyond  $1 + 1$  dimensions.

An elegant way of performing integrals with high dimensionality is to employ Monte Carlo techniques. Importance sampling is a prominent example in statistical field theory, though its formulation for fermionic fields is troublesome because of the Grassmann nature of these degrees of freedom. Nevertheless, there has been promising news to the apparently impossible simulations at finite chemical potential [63] or in real time [64].

In fact, the situation in our semiclassical nonequilibrium setting is much simpler than in Euclidean field theory simulations. We know everything about the initial fermion ensemble and we will set up evolution equations for the members of this ensemble. At any later time an averaging over these members will tell the propagator  $D(x, y)$ .

Notice that we could formulate Eqs. (6) and (7) as well as the backreaction (12)–(14) in Eq. (11) without any reference to the spectral function, which is complementary to the symmetrized propagator  $D(x, y)$ . We will replace the commutator of anticommuting operators by the product of plain complex numbers in  $D$ . To accept this simplification we have to show that the two-point function defined in terms of this simple product obeys the same equations of motion as  $D$  and that it also starts from the same initial condition.

Let us introduce a set of classical spinor stochastic variables as  $c$ -number fields:  $\psi_M(x)$  and  $\psi_F(x)$ . Only together can these “male” and “female” fields form a meaningful physical quantity, but the male and female roles are interchangeable:

$$D(x, y) = \langle \psi_M(x) \bar{\psi}_F(y) \rangle = \langle \psi_F(x) \bar{\psi}_M(y) \rangle. \quad (44)$$

The reason for why we need two spinor fields is that with a single spinor field only positive semidefinite correlators can be modeled, whereas  $\mathcal{M}(\vec{p})$  in Eq. (23) has negative eigenvalues.

So that  $D$  in Eq. (44) obeys Eqs. (6) and (7) we require that both the male and female stochastic spinors follow the usual Dirac equation:

$$(i\gamma^\mu \partial_\mu - m + g \operatorname{Re}\Phi(x) - ig \operatorname{Im}\Phi(x)\gamma^5)\psi_g(x) = 0. \quad (45)$$

The  $g$  (gender) index represents  $M$  or  $F$ .

The currents expressed in terms of the stochastic fields read

$$J^S(x) = g \operatorname{Tr}D(x, x) = g \langle \psi_F^+(x) \gamma^0 \psi_M(x) \rangle, \quad (46)$$

$$J^{\text{PS}}(x) = g \operatorname{Tr}D(x, x) \gamma^5 = g \langle \psi_F^+(x) \gamma^0 \gamma^5 \psi_M(x) \rangle. \quad (47)$$

Because of the interchangeability of  $\psi_M$  and  $\psi_F$  the scalar and pseudoscalar currents are manifestly real and imaginary, respectively.

We have to make sure to satisfy Eq. (15). For this we define the Fourier transformed stochastic fields:

$$\psi_g(\vec{p}) = \int_{\vec{x}} e^{i\vec{p}\cdot\vec{x}} \psi_g(\vec{x}), \quad \psi_g(\vec{x}) = \int_{\vec{p}} e^{-i\vec{p}\cdot\vec{x}} \bar{\psi}_g(\vec{p}). \quad (48)$$

To reproduce Eq. (15) we require

$$\langle \psi_M(\vec{p}) \psi_F^+(\vec{q}) \rangle = (2\pi)^3 \delta(\vec{p} - \vec{q}) \frac{1}{2} \mathcal{M}(\vec{p}). \quad (49)$$

To actually realize an initial ensemble with this correlator one has to solve the eigenvalue problem of  $\mathcal{M}(\vec{p})$ . This we have actually done already when we introduced the mode functions and denoted the eigenspinors as  $u^{(1)}$ ,  $u^{(2)}$ ,  $v^{(1)}$ , and  $v^{(2)}$  corresponding to the eigenvalues  $+1$ ,  $+1$ ,  $-1$ , and  $-1$ , respectively.

We can express the stochastic spinor fields in terms of the eigenspinors as follows:

$$\psi_{M,F}(\vec{p}) = \frac{1}{\sqrt{2}} \sum_s (\xi_s(\vec{p}) u^s(\vec{p}) \pm \eta_s(\vec{p}) v^s(\vec{p})). \quad (50)$$

$\xi^s$  and  $\eta^s$  are the primary complex random variables we use:

$$\begin{aligned} \langle \xi^s(\vec{p}) \xi^{s'}(\vec{p})^+ \rangle &= (2\pi)^3 \delta(\vec{p} - \vec{q}) \delta_{s,s'} (1 - 2n_+^s(\vec{p})), \\ \langle \eta^s(\vec{p}) \eta^{s'}(\vec{p})^+ \rangle &= (2\pi)^3 \delta(\vec{p} - \vec{q}) \delta_{s,s'} (1 - 2n_-^s(\vec{p})). \end{aligned}$$

All other two-point correlators vanish. (Actually, these variables could be chosen real and do not necessarily have to be Gaussian.) Notice that nothing on the right-hand side of Eq. (50) bears a gender index, but the male and female fields have different signs for the antiparticle component. This allows for the stochastic representation of the Hermitian matrix with negative eigenvalues in Eq. (49). With  $\xi$  and  $\eta$  we actually simulate the ladder operators; this is possible since the ladder operators always appear in the expectation value of a commutator.

The eigenvalues of the correlator  $\langle \psi_M(\vec{p}) \psi_F^+(\vec{p}) \rangle$ , which is a matrix in Dirac indices, actually represent the particle number: they take the value  $\frac{1}{2} - n_+^{(s)}(\vec{p})$  for the fermions, and  $n_-^{(s)}(\vec{p}) - \frac{1}{2}$  for the antifermions. By proper initialization, one can start from a polarized fermion gas, or, one can set a constant nonvanishing baryon density, as we anticipated. In a completely symmetric setting we can read out the particle number by taking the determinant of the correlation matrix (in momentum space), which shall be  $(n(\vec{p}) - \frac{1}{2})^4$ .

At this point we return to the question of numerical feasibility. The expectation value in Eq. (44) turns into an average over  $E$  pairs of spinor fields in practice, where  $E$  is finite number. The statistical error in Eq. (44) propagates through Eqs. (12)–(14) into the scalar equation. The

statistical noise in the backreaction may induce artificial production of scalar fluctuations. Thus, checking for the  $E$  dependence of the final result is an essential part of using this scheme. If the required number of spinor pairs ( $E$ ) turns out to be higher than the number of lattice sites, the standard deterministic mode function expansion is the cheaper and more precise option. This is typically the case in  $1 + 1$  dimensions. Increasing the number of dimensions, however, one can in most cases keep  $E$  around the linear lattice size or less, and the stochastic method can be by several orders of magnitude more efficient than the deterministic algorithm, both in memory need and in time.

For future reference we give the actual form of the spinor equations as well as their initialization in Appendix A. Since the system we analyze is implicitly understood to be discretized on a lattice, some comments on lattice doublers are due in Appendix B.

#### IV. EFFECTIVE SCALAR DYNAMICS

In this section, we present the numerical analysis of a real scalar field coupled to fermions as introduced above. For the sake of simplicity of the implementation we restrict our numerics to  $2 + 1$  dimensions.

We perform the renormalization of the effective potential as already anticipated, but no wave function renormalization is necessary. In Fig. 1, we give  $\delta V'(\Phi)$  by evaluating the two-dimensional variant of Eq. (41) on a large lattice for various fermion masses. In the plot, we used  $a$  for the lattice spacing. Notice that in the massive case with broken chiral symmetry we loose the  $\Phi \leftrightarrow -\Phi$  symmetry. For this reason we use massless fermions and compensate for the doublers as detailed in Appendix B.

In the following, we discuss a few test cases to explore the capabilities of this semiclassical approximation. To

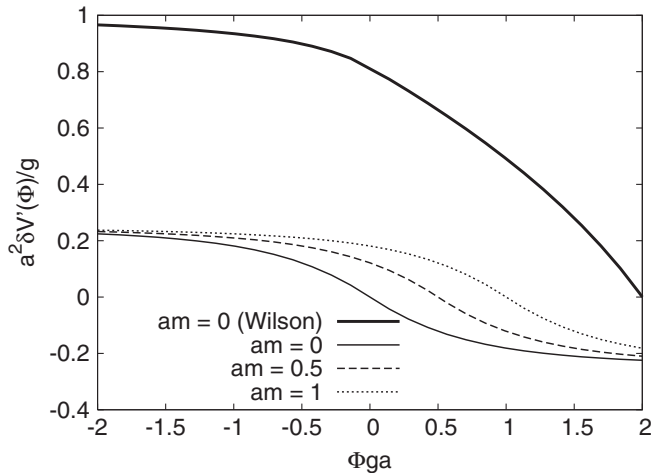


FIG. 1. Renormalization of the effective potential. For the thick line we used Wilson fermions in two spatial dimensions with  $r = 1$ . The other lines have been calculated in the presence of doublers. The breaking of chiral symmetry manifests in the asymmetry of  $\delta V'(\Phi)$  around zero.

better see the effects of the fermions we always run the purely classical simulation with the same initial condition (same random seed) in parallel. For reproducibility we give the parameters in the figure captions: the linear lattice size ( $N$ ), the Yukawa coupling ( $g$ ), the fermion's initial temperature ( $T_f$ ), the scalar mass ( $\mu$ ) and coupling ( $\lambda$ ), and the number of spinor fields ( $E$ ) in the ensemble. In these experiments we used two-component chiral fermions. These parameters and the data on the plots are given in lattice units (with  $a = 1$ ).

In our first exercise, we plot the damping of the scalar homogeneous mode in Fig. 2. The exponential with expected rate ( $\gamma = g^2/16$  in  $2 + 1$  dimensions with two-component spinors) nicely forms an envelope of the calculated evolution. It was important to use a large volume, otherwise the damping stopped at about  $N/2$  time and recurrences occur. In fact, one assumes infinite volume in the derivation of the decay rate.

Let us now consider an example where the fermions start from a finite temperature state and transfer energy to the bosonic vacuum. We set up an experiment with a small noise in the bosonic sector,  $\mu^2 = 0.25$ ,  $\lambda = 6$ ,  $g = 0.25$ , and  $T_f = 1$ . To our surprise, there was no boson production at all, but the small initial scalar noise was transformed into fermions with a rate comparable to  $\gamma$ . It seems that in the semiclassical approximation the production of quantum fluctuation is a one-way channel of interaction.

To see how the energy is transferred to fermions regardless of our thermodynamical preconceptions, we present the results of our third experiment. The scalar field is now started from a nonthermally excited state with an isotropic particle distribution peaked around the momenta  $|\vec{k}_0| = 0.5$  with  $n(|\vec{k}_0|) = 10$ . The initial energy density was  $\approx 1$ . What we see in Fig. 3 is a counterintuitive antithermalization, where all energy that can be possibly transformed to quantum fluctuations is taken away from the background.

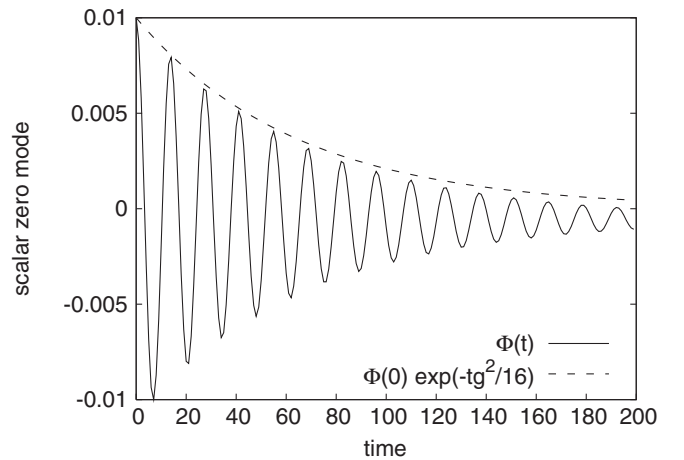


FIG. 2. The homogeneous mode of the scalar field is exponentially damped at the expected rate. (Parameters:  $N = 1024$ ,  $g = 0.5$ ,  $T_f = 0$ ,  $\mu^2 = 0.25$ ,  $\lambda = 0$ , and  $E = 20$ ).

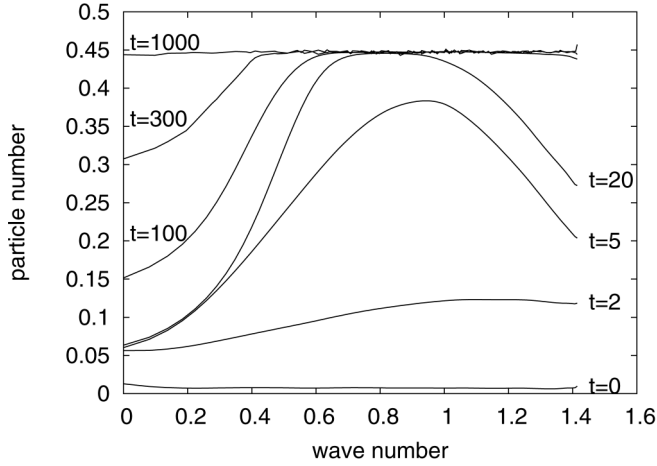


FIG. 3. Antithermalization. The bosonic excitations are transformed to fermions until fermion production is cut by Pauli blocking and a close-to-infinity temperature sets in. (Parameters:  $N = 64$ ,  $g = 0.5$ ,  $T_f = 0$ ,  $\mu^2 = 0.25$ ,  $\lambda = 24$ , and  $E = 32$ . We averaged the spectra from 20 runs.)

This also happens in the purely bosonic Hartree approximation, but here in the fermionic case the particle number is capped at a value close to  $1/2$  due to Pauli blocking. The modes above  $|\vec{k}| > 1$  are quickly excited (at the order of damping time). The low momentum modes are filled up on a much slower scale. At this point we remark that a two-dimensional classical scalar theory comes into nonthermal (quasi) fixed points for a wide range of initial conditions. For a similar classical system we found that the evolution to equilibrium can be extremely slow, governed by a power law [65]. In this example, too, the scalar spectrum evolves into an approximate power law with an exponent of  $\approx -1.8(2)$ . The effects of fermions manifest merely as an overall coefficient in the spectrum.

To gain more insight into the counterintuitive thermodynamics of this semiclassical system we tuned our numerical experiment to extremes: We started our system with thermal fermions and set zero initial scalar occupancy. We implemented this as a small white noise with negligible energy density. In this setting, the fermions were started from temperature 1 whereas the kinetic temperature of the scalar background was 0.002 in lattice units. Even in this case there was no energy transfer from the fermionic fluctuations to the scalars, but the scalar noise itself exhibited a decay. Starting the bosonic field from exactly zero, its kinetic temperature immediately rose to  $10^{-6}$  and decayed on a similar time scale as before. Whether the scalar energy density converges to zero or a finite value we could not determine from our present numerics.

We finally show an example where the classical approximation is expected to work well. We start the classical system from the center of a double-well potential. There is a rapid particle production fueled by the spinodal instability. The resulting scalar spectrum is not far from a Bose-

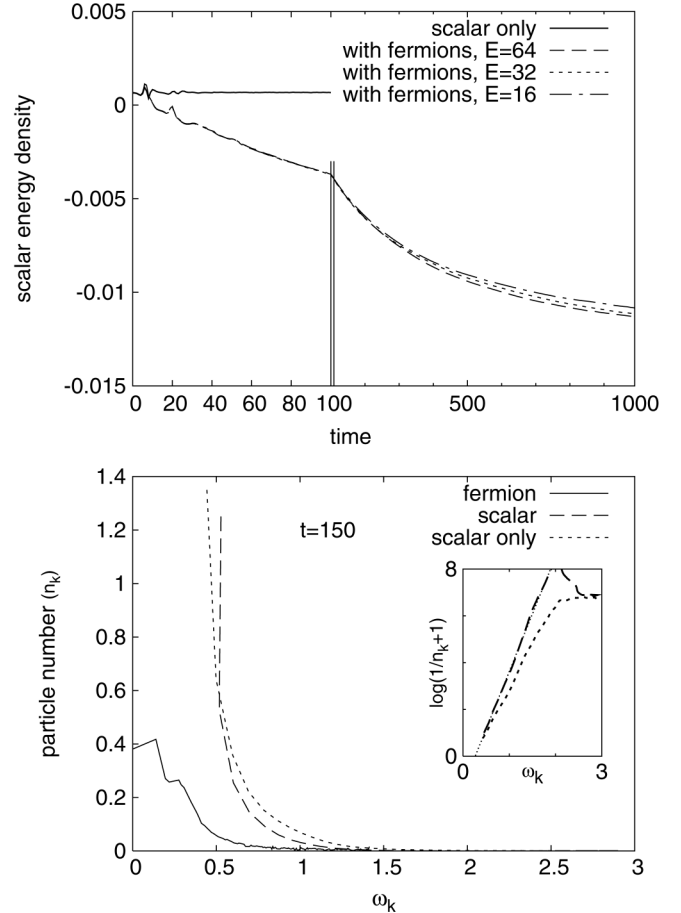


FIG. 4. Scalar field with a spinodal instability. *Top*: energy density of the scalar field with or without coupling to fermions. For comparison we show results at three different ensemble sizes. *Bottom*: the particle spectra at  $t = 150$ . At and around the time shown, the scalar spectrum is close to the Bose-Einstein distribution, especially when coupled to fermions. The dotted line in the inset plot is the thermal fit ( $\beta = 4.9$ ). (Parameters:  $N = 64$ ,  $g = 0.25$ ,  $T_f = 0$ ,  $\mu^2 = -0.25$ ,  $\lambda = 6$ , and  $E = 64, 32, 16$ . We averaged the spectra from 20 runs.)

Einstein distribution. Of course, this closeness to quantum equilibrium is temporary: the slow classical thermalization drives the system towards classical equipartition. Coupling this scalar field to fermions switches on a dissipation, as one can see in the plotted energy density in Fig. 4.

The scalar spectra in Fig. 4 are close to a quantum equilibrium distribution with some chemical potential. The UV end of the spectrum is distorted by lattice artefacts, but otherwise the linear fit of  $\log(1/(n(\vec{p}) + 1))$  is adequate (see dotted line in Fig. 4). The closeness to the quantum equilibrium distribution is maintained throughout the time we followed the dynamics. The energy drain of the fermion field does not bring the scalars out of this equilibrium but imposes a steady cooling.

These numerical experiments lead us to the negative conclusion that the energy transfer between the classical

and quantum degrees of freedom is unidirectional. As it is also known, the produced quantum particles do not scatter on each other, and the energy transfer between modes through the inhomogeneous background is inefficient. Can this semiclassical approximation be used then at all?

We do think that in some circumstances this low-cost solution to add fermions to a classical field simulation is adequate. The rate of fermion production is correctly given account for, albeit these particles will not thermalize. The very mechanism of particle production and the simultaneous loss of energy in the bosonic sector is well described as long as fermions are not created in such an abundance that their nonthermal distribution could have impact on the backreaction. In fact, bulk observables, such as the scalar effective potential, prethermalize [66], i.e their value before thermalization can be used as an estimate to what one would find after equilibration. Even if the fermion distribution is nonphysical, the evolution of the bosonic background can be well approximated. If, however, the backscattering of the produced fermions to bosons becomes relevant, this semiclassical approximation will no longer be applicable. One can actually monitor the fermion particle numbers to check for relevance of (the absence of) backscattering.

## V. FERMIONIC DECAY OF OSCILLONS

We can consider the semiclassical approximation safe if the resulting fermion energy density is small. However, one of the justifications for the classical approximation is the high bosonic occupancy, which will inevitably generate an energy transfer into the fermionic fields. In such cases the approximation will break down within a short time, which is likely to be the damping time we discussed in the previous section.

In this section, we turn to applications where classicality has another justification. If the particle content is very low and there is dilute network of classical structures, such as topological defects, their evolution can be well described by the nonlinear wave equations. The decay of these structures into particles is mapped to the production of classical waves (“ripples”) by the classical equations. As this mostly happens in the ultraviolet, the classical approach is not justified for describing particle production, in contrast to its usefulness in the case of the macroscopic networks, like cosmic strings.

We addressed this deficiency of the classical approximation in Ref. [67], where we introduced a stochastic approach to the bosonic mean-field approximation, similar to the method presented in this paper. We found that mimicking the quantum distribution by an analogous classical noise (following the so-called “just-the-half” prescription) introduces undesired time-dependent renormalization effects to the effective potential. Instead we solved the inhomogeneous mean-field equations and found that on the macroscopic level, the decay channel into

quantum particles plays a negligible role, whereas on the microscopic scale we found deviations. Our numerical analysis suggested that oscillons, which are one of the classical decay products of topological defects [68], are the primary sources of quantum particles, while the direct radiative decay of a defect network is suppressed as predicted in Ref. [69].

To better understand how oscillons decay quantum mechanically we reproduce one of the experiments in Ref. [68], but we also add fermions. In two dimensions, oscillons are particularly stable [70,71] localized structures; when several oscillons are created in volume, they behave as molecules in a gas. When oscillons collide, they coalesce with some probability. This mechanism being their only decay process (in  $2 + 1$  dimensions), the number density of oscillons obeys the equation  $\dot{n}(t) \sim -n^2(t)$ . Thus, the classical solution is  $n(t) \sim 1/t$ , which is approximately manifest in classical simulations [68].

We put 16 incoherent oscillons with small random velocities in a box with  $N = 128$ . We estimate the number of oscillons by counting the sites with an energy density beyond a threshold ( $\epsilon > 0$ ). This number we normalize to its initial value and plot in Fig. 5. It takes long before the expected power-law solution sets in (and even then finite volume effects can distort it). But a small coupling to the fermionic fields introduces a new time scale, and the slow classical behavior is replaced by a close-to-exponential decay. (The oscillon damping rate is about 4 times stronger than for the homogeneous mode.) This process reduces the amplitude of most oscillons below the threshold. After

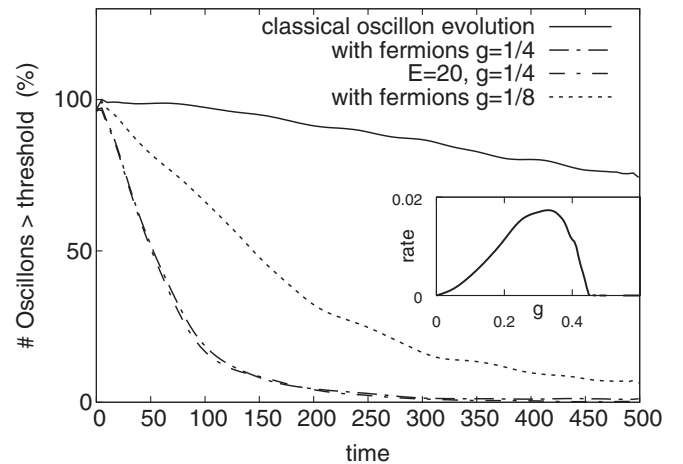


FIG. 5. Estimated “molecule” number in a gas of oscillons. When the scalar background is coupled to fermions, the slow classical evolution is replaced by an approximately exponential decay. An estimate of the rate as a function of the Yukawa coupling is shown in the inset plot. To obtain the same curves using the mode function expansion would have required 3 orders of magnitude more computational resources. For  $g = 1/4$  we explicitly check for the insensitivity to doubling the ensemble. (Parameters:  $N = 128$ ,  $T_f = 0$ ,  $\mu^2 = -0.25$ ,  $\lambda = 3$ , and  $E = 10$  or  $20$ . For each coupling we averaged 30 runs.)

$t > 100$ , however, the plotted estimate can be best fit by a power law with an exponent of  $-2$ . For the semiclassical evolution of these localized objects a surprisingly small spinor ensemble already provides results that are insensitive to an increase in  $E$ .

In the inset plot of Fig. 5, we estimated the oscillon decay rate by the inverse time necessary to radiate away  $100 \exp(-1)$  percent of the oscillons. The rate cuts off at about  $g_{\text{cut}} \approx 0.45$ . One can explain this by simple kinematics. The effective mass of the produced fermions  $m_f = gv$ , where  $v = \sqrt{-6\mu^2/\lambda}$  is the vacuum expectation value of the background. The scalar mass in the broken phase is  $m_b = \sqrt{-2\mu^2}$ . It is not this bosonic mass that enters the kinematical relation but the oscillon frequency  $\omega_{\text{osc}}$ , so the condition for the decay is  $\frac{1}{2}\omega_{\text{osc}} > m_f$ . From  $g_{\text{cut}}$  we can tell the oscillon frequency:  $\omega_{\text{osc}}/m_b = 2g_{\text{cut}}\sqrt{3/\lambda} \approx 0.9$ . This estimate is in harmony with direct measurements [68].

In this paper, our aim is not to explore the parameter space, or to analyze the mechanisms oscillon decay. Instead, we put forward a low-cost technique to check existing and future analyses of defect evolution for fermionic quantum corrections, complementing work already done for bosonic ones [67]. We plan to investigate the evolution of cosmic strings for such contributions from quantum degrees of freedom in a future publication.

## VI. CONCLUSIONS

In this paper, we propose a low-cost integration scheme for the fermionic path integral, which leads to equations that are equivalent to the mean-field approximation studied earlier by Aarts and Smit. These equations also follow from the large- $N_f$  expansion of the 2PI effective action. The computational efficiency of this scheme allowed us to do simulations beyond  $1 + 1$  dimensions. This stochastic method is a generalization of our earlier technique developed for scalars in Ref. [67].

Using a simple scalar field theory, we calculate several test cases and study what irreversible phenomena can be captured by this simple method. We confirm that the fermions, once created, can no longer scatter on each other, but this is not the only obstacle that hinders thermalization. The damping of the classical oscillations are correctly accounted for, but the backscattering of the fermions into bosons is absent. In the language of the mode function expansion, fermions (and also other quantum fluctuations on the Hartree level) are represented by far more dynamical variables than the background. If these variables strive for classical equipartition (as usual in a coupled set of nonlinear differential equations), the energy left in the background is negligible. This suppression of the background becomes stronger with higher dimensionality, and was less relevant in former  $1 + 1$  dimensional calculations.

As it was remarked in Ref. [52], the fermion spectrum can become close to thermal, and this raised hope that the

inhomogeneous Hartree approximation is still capable to account for an approximate thermalization. It is, however, more likely, that it is the particle production mechanism that brings the fermions close to equilibrium, rather than scattering.

Even though scattering cannot drive the fermions towards equilibrium, we expect that the backreaction of the often not-far-from-thermal fermion field has an approximately thermal backreaction due to prethermalization of the fermionic current [66], and the lack of thermalization has little impact on the background field. This assumption becomes even more plausible if we assume that the fermions leave the scene, once created.

In some physical situations it is difficult for a fermion to leave. If we apply the presented scheme to the Yang-Mills equations, and solve the semiclassical chromodynamics, it will be difficult for fermions to be reabsorbed by the plasma. This puts jet quenching outside of the range of validity. But a semiclassical simulation of the freeze-out of the plasma is not ruled out by the aforementioned deficiencies.

The numerical calculation of the fermion spectrum in baryogenesis scenarios is a more viable application. If baryogenesis is driven by a first order phase transition, the presented equations can account for  $CP$  violation as well as the departure from equilibrium without relying on gradient expansion, and thus, allowing for thin walls. For the subsequent thermalization, however, one has to make further assumptions.

The scheme is best applicable for systems with low particle numbers and genuine inhomogeneities, like a dilute network of topological defects, such as cosmic strings. In this context fermion production is local, and the produced particles spread in space. This results in small particle numbers, and we expect that the lack of thermalization will introduce very little distortion into the backreaction.

In conclusion, for cases where the inhomogeneities in the background are meant to be “particles,” a big volume is less relevant, and other techniques, such as the 2PI effective action on a homogeneous ensemble may be more favorable. For the large-scale classical simulations with inhomogeneous classical structures, however, the inhomogeneous 2PI approach would be beyond feasibility. In such situations, the Hartree approximation already includes the leading quantum corrections, and endorses fermions. The technique in this paper has made these type of calculations affordable.

## ACKNOWLEDGMENTS

The authors acknowledge the collaboration with Petja Salmi on a related project. The numerical work has been carried out on the Archimedes cluster of the University of Sussex. S. B. is funded by STFC.

## APPENDIX A: REPRESENTATION OF THE SPINOR FIELDS

The initial conditions for the spinor fields is given in terms of the  $u^s(\vec{p})$  and  $v^s(\vec{p})$  eigenspinors. Here, we present the actual form of these eigenvectors. We use the normalization factors for a theory discretized in a volume  $V$ .

The formulas are based on a naive fermion action. They can, however, be easily rewritten for the Wilson fermions by replacing  $m$  to  $m + \frac{1}{2}\hat{p}^2$  when discussing the  $\vec{p}$  mode, with  $\hat{p}_j = \frac{2}{a} \sin p_j a/2$ .

### 1. Chiral basis in 3 + 1 dimensions

In the chiral base we define the gamma matrices as

$$\gamma^0 = \begin{pmatrix} 0 & 1 \\ 1 & 0 \end{pmatrix}, \quad \gamma^i = \begin{pmatrix} 0 & \sigma^i \\ -\sigma^i & 0 \end{pmatrix},$$

$$\gamma^5 = \begin{pmatrix} -1 & 0 \\ 0 & 1 \end{pmatrix}.$$

Consequently,

$$\gamma^i \gamma^0 = \begin{pmatrix} \sigma^i & 0 \\ 0 & -\sigma^i \end{pmatrix}, \quad \gamma^0 \gamma^5 = \begin{pmatrix} 0 & 1 \\ -1 & 0 \end{pmatrix}. \quad (\text{A1})$$

The Hermitian 4-by-4 matrix in Eq. (49) in the chiral basis reads

$$\langle \psi_M(\vec{p}) \psi_F^\dagger(\vec{p}) \rangle = \frac{V}{2\omega_{\vec{p}}} \begin{pmatrix} \vec{p} \cdot \vec{\sigma} & m \\ m & -\vec{p} \cdot \vec{\sigma} \end{pmatrix}. \quad (\text{A2})$$

Here,  $\vec{p} \cdot \vec{\sigma}$  stands for the combination of the Pauli matrices:

$$\partial_0 \psi_g(x) = \begin{pmatrix} \partial_3 & \partial_1 - i\partial_2 & -iM_x^* & 0 \\ \partial_1 + i\partial_2 & -\partial_3 & 0 & -iM_x^* \\ -iM_x & 0 & -\partial_3 & -\partial_1 + i\partial_2 \\ 0 & -iM_x & -\partial_1 - i\partial_2 & \partial_3 \end{pmatrix} \psi_g(x) \quad (\text{A5})$$

with  $M_x = m - g\Phi(x)$ . We can use this equation for both  $\psi_M$  and  $\psi_F$ . For Wilson fermions  $M_x \rightarrow M_x - \frac{1}{2}\Delta$ .

### 2. Majorana basis in 2 + 1 dimensions

Here, we work out the implementation details for a 2 + 1 dimensional setting with a real scalar background. In 2 + 1 dimensions we have 2-by-2 gamma matrices. In Majorana basis all these are imaginary:

$$\gamma^0 = \begin{pmatrix} 0 & -i \\ i & 0 \end{pmatrix}, \quad \gamma^1 = \begin{pmatrix} i & 0 \\ 0 & -i \end{pmatrix},$$

$$\gamma^2 = \begin{pmatrix} 0 & i \\ i & 0 \end{pmatrix}.$$

In 2 + 1 dimensions one of the gamma matrices can be easily expressed by others:

$$\vec{p} \cdot \vec{\sigma} = \begin{pmatrix} \bar{p}_3 & \bar{p}_1 - i\bar{p}_2 \\ \bar{p}_1 + i\bar{p}_2 & -\bar{p}_3 \end{pmatrix}. \quad (\text{A3})$$

We used the standard notation  $\bar{p}_j = a \sin p_j a$ .

In the chiral base the eigenvectors are given as

$$u^{(1)} = \alpha \begin{pmatrix} |\vec{p}| + \omega_{\vec{p}} \\ m \end{pmatrix} \otimes \chi_p^+,$$

$$u^{(2)} = \alpha \begin{pmatrix} m \\ |\vec{p}| + \omega_{\vec{p}} \end{pmatrix} \otimes \chi_p^-,$$

$$v^{(1)} = \alpha \begin{pmatrix} -m \\ |\vec{p}| + \omega_{\vec{p}} \end{pmatrix} \otimes \chi_p^+,$$

$$v^{(2)} = \alpha \begin{pmatrix} |\vec{p}| + \omega_{\vec{p}} \\ -m \end{pmatrix} \otimes \chi_p^-,$$
(A4)

with  $\alpha^2 = \frac{1}{2\omega_{\vec{p}}(\omega_{\vec{p}} + |\vec{p}|)}$ .  $\chi^\pm(\vec{p})$  denotes the eigenvectors of  $p_i \sigma^i$  for the eigenvalues  $|\vec{p}|$  and  $-|\vec{p}|$ , respectively.

Let us now diagonalize  $p_j \sigma^j$ :

$$\chi_p^+ = \beta_+ \begin{pmatrix} p_3 + |\vec{p}| \\ p_1 + ip_2 \end{pmatrix} \chi_p^- = \beta_+ \begin{pmatrix} -p_1 + ip_2 \\ p_3 + |\vec{p}| \end{pmatrix} \quad \text{if } p_3 > 0;$$

$$\chi_p^+ = \beta_- \begin{pmatrix} p_1 - ip_2 \\ |\vec{p}| - p_3 \end{pmatrix} \chi_p^- = \beta_- \begin{pmatrix} p_3 - |\vec{p}| \\ p_1 + ip_2 \end{pmatrix} \quad \text{if } p_3 < 0$$

with  $\beta_\pm^2 = 1/2|\vec{p}|(|\vec{p}| \pm p_3)$ . The two cases we handle separately for numerical stability (e.g. to avoid divisions by zero).

We actually solve the Dirac equation (45) for the  $\psi_g$  field instances. This reads in chiral base

$$\gamma^0 \gamma^1 = i\gamma^2, \quad \gamma^0 \gamma^2 = -i\gamma^1. \quad (\text{A6})$$

The Dirac equation in this basis (with  $M_x = m - g\Phi$ ) reads

$$\partial_0 \psi = \begin{pmatrix} -\partial_2 & \partial_1 - M_x \\ \partial_1 + M_x & \partial_2 \end{pmatrix} \psi. \quad (\text{A7})$$

The advantage of the Majorana basis becomes apparent with the form of this equation: the spinor field equation is real. Although the spinor fields themselves are complex, their real and imaginary parts follow a separate equation of motion. This facilitates numerical optimizations, such as vectorized arithmetic, and it requires a smaller memory-to-cache bandwidth.

We have to initialize the spinors in terms of eigenspinors. For this, we diagonalize the vacuum correlation matrix

$$\mathcal{M}(\vec{p}) = \frac{1}{\omega_{\vec{p}}} \begin{pmatrix} -\bar{p}_2 & \bar{p}_1 - im \\ \bar{p}_1 + im & \bar{p}_2 \end{pmatrix}. \quad (\text{A8})$$

One finds that the eigenvectors are

$$u(\vec{p}) = \beta \begin{pmatrix} Q^* \\ s \end{pmatrix}, \quad v(\vec{p}) = \beta \begin{pmatrix} -s \\ Q \end{pmatrix}, \quad (\text{A9})$$

for  $p_2 > 0$ , and

$$u(\vec{p}) = \beta \begin{pmatrix} -s \\ Q \end{pmatrix}, \quad v(\vec{p}) = \beta \begin{pmatrix} Q^* \\ s \end{pmatrix}, \quad (\text{A10})$$

with  $Q = \bar{p}_1 - im$ ,  $s = \bar{p}_2 + \omega_{\vec{p}}$ , and  $\beta^{-2} = |Q|^2 + s^2$ .

## APPENDIX B: FERMION DOUBLING PROBLEM IN THE SEMICLASSICAL THEORY

The problem of fermion doubling inevitably arises in any lattice implementation. Since almost all numerical analyses of classical field theories use lattice discretization, an extension that incorporate fermions will also share this heritage. Time discretization, however, is not an intrinsic parameter of the classical theory. Whereas the spacelike continuum limit simply does not exist, we can always assume that our equations are in the timelike continuum limit. Indeed, the time step ( $a_t$ ) in our numerics was much smaller than the lattice spacing  $a = 20a_t$ .

There are several remedies in the literature for the problem of doublers. We made a version of our numerics using Wilson fermions, but the explicit breaking of chiral symmetry introduced a linear term in the potential. Although this can be renormalized away, not only the vacuum, but also the physical excitations will also contribute and introduce artefacts in the scalar effective potential. This effect will vanish in the continuum limit, but in a semiclassical theory, we cannot go close to the continuum limit, by construction.

The other low-cost solution could be the use of staggered fermions. These are, however, special to two or four dimensions, and some of the doublers will be kept. To avoid complications on the level of the equation of motion we dropped this idea too.

In the presented numerics we simply used the naive fermion discretization and introduce an effective flavor number, in which we compensate for a pair of doublers in each spatial direction. We could do this since in our simple model there are no anomalous diagrams where doubling fermions could cancel.

There is, however, a timelike discretization, too, which can be a source of timelike doublers. To eliminate them, Aarts and Smit used a linear combination of two different flavors, and the 2 degrees of freedom have both been made physical.

In the following we analyze the real-time Dirac equation to understand how such doublers affect our numerics.

The free Dirac propagator on spatial lattice in momentum space reads

$$D(t, \vec{p}) = \frac{m + \bar{p}_j \gamma^j}{2\omega_{\vec{p}}} \cos(\omega t) - i \frac{\gamma^0}{2} \sin(\omega t) \quad (\text{B1})$$

with  $\bar{p}_j = a^{-1} \sin(ap_j)$  and  $\omega_{\vec{p}}^2 = m^2 + \sum_j \bar{p}_j^2$ . In the timelike continuum limit  $\omega = \omega_{\vec{p}}$  must be satisfied so that Eq. (B1) solves the Dirac equation. If time is discretized as the average of the forward and backward derivative, then Dirac equation takes the following form:

$$\left( \frac{i}{2} \gamma^0 [\nabla_t^f + \nabla_t^b] + \gamma^j \bar{p}_j - m \right) D(t, \vec{p}) = 0. \quad (\text{B2})$$

Inserting Eq. (B1) into Eq. (B2) we get following constraint:  $\bar{\omega} = \omega_{\vec{p}}$  with  $\bar{\omega} = a_t^{-1} \sin(\omega a_t)$ . For an extremely anisotropic lattice ( $a_t \ll a$ ) either  $\bar{\omega} \approx \omega$  or  $\bar{\omega} \approx \pi/a_t - \omega$ , since  $\omega_{\vec{p}}$  is limited by the spatial cutoff. This means, that there are two solutions (the doublers) which can be worked out explicitly as

$$D_1(t, \vec{p}) = \frac{m + \bar{p}_j \gamma^j}{2\omega_{\vec{p}}} \cos(\omega_{\vec{p}} t) - i \frac{\gamma^0}{2} \sin(\omega_{\vec{p}} t), \quad (\text{B3})$$

$$D_2(t, \vec{p}) = \frac{m + \bar{p}_j \gamma^j}{2\omega_{\vec{p}}} \cos(\omega_{\vec{p}} t) (-1)^s - i \frac{\gamma^0}{2} \sin(\omega_{\vec{p}} t) (-1)^{s+1}, \quad (\text{B4})$$

where  $s$  is the index of the time slice  $t$ , i.e.  $t = a_t s$ . The sum of these solutions is the standard lattice propagator:

$$D_{\text{lat}}(t, \vec{p}) = 2 \left[ \frac{m + \bar{p}_j \gamma^j}{2\omega_{\vec{p}}} \cos(\omega_{\vec{p}} t) \chi_e(s) - i \frac{\gamma^0}{2} \sin(\omega_{\vec{p}} t) \chi_o(s) \right], \quad (\text{B5})$$

where we introduced the  $\chi_e()$  and  $\chi_o()$  functions, which is one if their integer argument is even or odd, respectively, and zero otherwise. Indeed, Fourier transforming Eq. (B5) yields (in the  $a_t/a \ll 1$  limit)

$$D_{\text{lat}}(p) = \pi \delta(\bar{p}_0^2 - \omega_{\vec{p}}^2) [(m + \bar{p}_j \gamma^j) + \gamma^0 \omega_{\vec{p}} \text{sgn}(\bar{p}_0)]. \quad (\text{B6})$$

We get the continuum propagator from Eq. (B6) by removing the bars. The staggered nature of the lattice propagator is also manifest in spatial coordinates: e.g.  $\text{Tr} D(t, \vec{x}) \gamma^1$  is only then nonvanishing if  $x_1/a$  is odd.

If we use the  $D_{\text{lat}}$  in the equations, the  $\chi_e()$  function will always give one in the source  $J$ , since there we close the Fermion loop by evaluating the propagator equal space and time. At that point we need to compensate for the extra factor of 2, compared to the continuum limit. We achieve this by removing a factor of 2 in Eq. (B5) from the initial value of  $D$ .

At zero time we start our system with excitations described by the  $D_1$  propagator. The space and time-dependence of the background will result an inhomoge-

neous propagator  $D_1(x, y)$ . Had we started from an initial condition corresponding to the  $D_2$  propagator, the evolution would have led to  $D_2(x, y)$ . Inserting  $D_{\text{lat}} = D_1(x, y) + D_2(x, y)$  or  $\bar{D}_{\text{lat}} = D_1(x, y) - D_2(x, y)$  into the inhomogeneous Dirac equation one discovers that these linear combinations decouple: they communicate only through the backreaction to the scalars. The various Lorentz components of  $D_{\text{lat}}(x, y)$  and  $\bar{D}_{\text{lat}}(x, y)$  couple to the background at different time slices, depending on the parity of  $x^0 - y^0$ . If the background is a smooth function of time,  $D_{\text{lat}}$  and  $\bar{D}_{\text{lat}}$  will evolve on the same background, up to an error  $\sim a_t$ . Thus, their difference,  $D_2(x, y)$  is suppressed by the timelike spacing, i.e. if there is no  $D_2$  component in our initial condition, the production of dou-

bler particles will be small compared to the standard particles. In the backreaction and the measured spectra both types of excitations contribute indistinguishably. (Notice that  $D_1(t, \vec{p})$  and  $D_2(t, \vec{p})$  are identical at equal time, where these observables are taken.) Similar ideas have been implemented to tackle the species doubling problem in the context of the hard thermal loop effective action of the electroweak theory in Ref. [72].

To check these ideas we plotted the damping of the scalar field in Fig. 2. For this calculation in  $2 + 1$  dimensions we used the effective flavors number  $1/4$ . An erroneous estimation of the number of flavors should have generated an unexpected factor of 2 in the rate.

- 
- [1] J. H. Traschen and R. H. Brandenberger, Phys. Rev. D **42**, 2491 (1990); Y. Shtanov, J. H. Traschen, and R. H. Brandenberger, Phys. Rev. D **51**, 5438 (1995).
  - [2] L. Kofman, A. D. Linde, and A. A. Starobinsky, Phys. Rev. Lett. **73**, 3195 (1994); Phys. Rev. D **56**, 3258 (1997).
  - [3] S. Khlebnikov, L. Kofman, A. D. Linde, and I. Tkachev, Phys. Rev. Lett. **81**, 2012 (1998).
  - [4] T. W. B. Kibble, J. Phys. A **9**, 1387 (1976); M. B. Hindmarsh and T. W. B. Kibble, Rep. Prog. Phys. **58**, 477 (1995).
  - [5] A. Vilenkin and E. P. S. Shellard, *Cosmic Strings and Other Topological Defects* (Cambridge University Press, Cambridge, 1994).
  - [6] I. Tkachev, S. Khlebnikov, L. Kofman, and A. D. Linde, Phys. Lett. B **440**, 262 (1998).
  - [7] A. Krasnitz and R. Venugopalan, Phys. Rev. Lett. **86**, 1717 (2001).
  - [8] S. Y. Khlebnikov and I. I. Tkachev, Phys. Rev. Lett. **77**, 219 (1996); G. N. Felder and L. Kofman, Phys. Rev. D **63**, 103503 (2001).
  - [9] A. Chambers and A. Rajantie, Phys. Rev. Lett. **100**, 041302 (2008); J. Cosmol. Astropart. Phys. 08 (2008) 002.
  - [10] S. Y. Khlebnikov and I. I. Tkachev, Phys. Rev. D **56**, 653 (1997).
  - [11] A. Nicolis, Classical Quantum Gravity **21**, L27 (2004); C. Grojean and G. Servant, Phys. Rev. D **75**, 043507 (2007).
  - [12] J. Garcia-Bellido and D. G. Figueroa, Phys. Rev. Lett. **98**, 061302 (2007); J. Garcia-Bellido, D. G. Figueroa, and A. Sastre, Phys. Rev. D **77**, 043517 (2008).
  - [13] A. Diaz-Gil, J. Garcia-Bellido, M. Garcia Perez, and A. Gonzalez-Arroyo, Phys. Rev. Lett. **100**, 241301 (2008); A. Diaz-Gil, J. Garcia-Bellido, M. G. Perez, and A. Gonzalez-Arroyo, J. High Energy Phys. 07 (2008) 043.
  - [14] L. Kofman, A. D. Linde, and A. A. Starobinsky, Phys. Rev. Lett. **76**, 1011 (1996); G. N. Felder, J. Garcia-Bellido, P. B. Greene, L. Kofman, A. D. Linde, and I. Tkachev, Phys. Rev. Lett. **87**, 011601 (2001).
  - [15] J. Garcia-Bellido, D. Y. Grigoriev, A. Kusenko, and M. E. Shaposhnikov, Phys. Rev. D **60**, 123504 (1999);
  - [16] G. D. Moore and N. Turok, Phys. Rev. D **55**, 6538 (1997); G. D. Moore, J. High Energy Phys. 11 (2001) 021.
  - [17] A. Rajantie, P. M. Saffin, and E. J. Copeland, Phys. Rev. D **63**, 123512 (2001); A. Tranberg and J. Smit, J. High Energy Phys. 11 (2003) 016; A. Tranberg, J. Smit, and M. Hindmarsh, J. High Energy Phys. 01 (2007) 034; A. Tranberg, J. Smit, and M. Hindmarsh, Nucl. Phys. A **785**, 102 (2007).
  - [18] N. Bevis, M. Hindmarsh, M. Kunz, and J. Urrestilla, Phys. Rev. D **75**, 065015 (2007).
  - [19] P. Goddard, J. Goldstone, C. Rebbi, and C. B. Thorn, Nucl. Phys. **B56**, 109 (1973).
  - [20] G. Vincent, N. D. Antunes, and M. Hindmarsh, Phys. Rev. Lett. **80**, 2277 (1998);
  - [21] J. N. Moore, E. P. S. Shellard, and C. J. A. Martins, Phys. Rev. D **65**, 023503 (2001);
  - [22] M. Yamaguchi, Phys. Rev. D **60**, 103511 (1999); M. Yamaguchi, J. Yokoyama, and M. Kawasaki, Phys. Rev. D **61**, 061301 (2000).
  - [23] A. Achucarro, P. Salmi, and J. Urrestilla, Phys. Rev. D **75**, 121703 (2007).
  - [24] J. Urrestilla, N. Bevis, M. Hindmarsh, M. Kunz, and A. R. Liddle, J. Cosmol. Astropart. Phys. 07 (2008) 010.
  - [25] T. Garagounis and M. Hindmarsh, Phys. Rev. D **68**, 103506 (2003).
  - [26] J. C. R. Oliveira, C. J. A. Martins, and P. P. Avelino, Phys. Rev. D **71**, 083509 (2005).
  - [27] N. Bevis, M. Hindmarsh, M. Kunz, and J. Urrestilla, Phys. Rev. Lett. **100**, 021301 (2008).
  - [28] T. Lappi, Phys. Rev. C **67**, 054903 (2003); F. Gelis, K. Kajantie, and T. Lappi, Phys. Rev. Lett. **96**, 032304 (2006); T. Lappi and L. McLerran, Nucl. Phys. A **772**, 200 (2006).
  - [29] F. Gelis and R. Venugopalan, Acta Phys. Pol. B **37**, 3253 (2006).
  - [30] S. Mrowczynski, Phys. Lett. B **314**, 118 (1993); A. Rebhan, P. Romatschke, and M. Strickland, Phys. Rev. Lett. **94**, 102303 (2005).
  - [31] P. Romatschke and R. Venugopalan, Phys. Rev. Lett. **96**,

- 062302 (2006); Phys. Rev. D **74**, 045011 (2006).
- [32] J. Berges, S. Scheffler, and D. Sexty, Phys. Rev. D **77**, 034504 (2008).
- [33] P. Arnold and G.D. Moore, Phys. Rev. D **73**, 025006 (2006); **76**, 045009 (2007).
- [34] D. Bodeker and K. Rummukainen, J. High Energy Phys. **07** (2007) 022.
- [35] Z. Szep, Ph.D. thesis, Eötvös University, Budapest, 2001, arXiv:hep-ph/0110024.
- [36] M. Gleiser, Phys. Rev. D **49**, 2978 (1994); E. J. Copeland, M. Gleiser, and H.R. Muller, Phys. Rev. D **52**, 1920 (1995).
- [37] M. Gleiser, B. Rogers, and J. Thorarinson, Phys. Rev. D **77**, 023513 (2008).
- [38] G. Aarts, B.J. Nauta, and C.G. van Weert, Phys. Rev. D **61**, 105002 (2000).
- [39] J. Berges, AIP Conf. Proc. **739**, 3 (2004).
- [40] J. Berges and J. Serreau, Phys. Rev. Lett. **91**, 111601 (2003).
- [41] J. Berges, A. Rothkopf, and J. Schmidt, Phys. Rev. Lett. **101**, 041603 (2008).
- [42] G. Aarts and J.M. Martinez Resco, J. High Energy Phys. **11** (2002) 022.
- [43] S. Borsanyi and U. Reinosa, Phys. Lett. B **661**, 88 (2008).
- [44] T. Gasenzer, J. Berges, M. G. Schmidt, and M. Seco, Phys. Rev. A **72**, 063604 (2005).
- [45] P. Aurenche, F. Gelis, and H. Zaraket, Phys. Rev. D **62**, 096012 (2000); P. Aurenche, F. Gelis, R. Kobes, and H. Zaraket, Phys. Rev. D **58**, 085003 (1998).
- [46] P. Arnold, G.D. Moore, and L.G. Yaffe, J. High Energy Phys. **01** (2003) 030.
- [47] A. Rajantie and A. Tranberg, J. High Energy Phys. **11** (2006) 020.
- [48] G. Aarts and J. Berges, Phys. Rev. Lett. **88**, 041603 (2002).
- [49] A. Arrizabalaga, J. Smit, and A. Tranberg, J. High Energy Phys. **10** (2004) 017.
- [50] J. Berges, S. Borsanyi, and J. Serreau, Nucl. Phys. **B660**, 51 (2003).
- [51] G. Aarts and J. Smit, Nucl. Phys. **B555**, 355 (1999).
- [52] G. Aarts and J. Smit, Phys. Rev. D **61**, 025002 (1999).
- [53] G. Gibbons, K. i. Maeda, and Y. i. Takamizu, Phys. Lett. B **647**, 1 (2007).
- [54] P.M. Saffin and A. Tranberg, J. High Energy Phys. **12** (2007) 053; **08** (2007) 072.
- [55] F. Cooper and E. Mottola, Phys. Rev. D **36**, 3114 (1987); F. Cooper, S. Habib, Y. Kluger, E. Mottola, J.P. Paz, and P.R. Anderson, Phys. Rev. D **50**, 2848 (1994).
- [56] D. Boyanovsky, H. J. de Vega, R. Holman, and J. Salgado, Phys. Rev. D **59**, 125009 (1999); F.J. Cao and H.J. de Vega, Phys. Rev. D **65**, 045012 (2002).
- [57] J. Baacke and K. Heitmann, Phys. Rev. D **62**, 105022 (2000); J. Baacke and S. Michalski, Phys. Rev. D **65**, 065019 (2002).
- [58] J. Baacke, K. Heitmann, and C. Patzold, Phys. Rev. D **58**, 125013 (1998); J. Baacke and C. Patzold, Phys. Rev. D **62**, 084008 (2000).
- [59] G.F. Giudice, M. Peloso, A. Riotto, and I. Tkachev, J. High Energy Phys. **08** (1999) 014.
- [60] J. Garcia-Bellido, S. Mollerach, and E. Roulet, J. High Energy Phys. **02** (2000) 034; J. Garcia-Bellido and E. Ruiz Morales, Phys. Lett. B **536**, 193 (2002).
- [61] M. Salle, J. Smit, and J.C. Vink, Phys. Rev. D **64**, 025016 (2001); Nucl. Phys. **B625**, 495 (2002); M. Salle and J. Smit, Phys. Rev. D **67**, 116006 (2003).
- [62] L.M.A. Bettencourt, K. Pao, and J.G. Sanderson, Phys. Rev. D **65**, 025015 (2001).
- [63] G. Aarts and I.O. Stamatescu, J. High Energy Phys. **09** (2008) 018.
- [64] J. Berges and I.O. Stamatescu, Phys. Rev. Lett. **95**, 202003 (2005); J. Berges, S. Borsanyi, D. Sexty, and I.O. Stamatescu, Phys. Rev. D **75**, 045007 (2007); J. Berges and D. Sexty, Nucl. Phys. **B799**, 306 (2008).
- [65] S. Borsanyi and Z. Szep, Phys. Lett. B **508**, 109 (2001).
- [66] J. Berges, S. Borsanyi, and C. Wetterich, Phys. Rev. Lett. **93**, 142002 (2004).
- [67] S. Borsanyi and M. Hindmarsh, Phys. Rev. D **77**, 045022 (2008).
- [68] M. Hindmarsh and P. Salmi, Phys. Rev. D **74**, 105005 (2006); **77**, 105025 (2008).
- [69] M. Srednicki and S. Theisen, Phys. Lett. B **189**, 397 (1987).
- [70] P.M. Saffin and A. Tranberg, J. High Energy Phys. **01** (2007) 030.
- [71] M. Gleiser and D. Sicilia, Phys. Rev. Lett. **101**, 011602 (2008).
- [72] D. Bodeker, G.D. Moore, and K. Rummukainen, Phys. Rev. D **61**, 056003 (2000).